Clathrin-inspired coating and stabilization of liposomes by DNA self-assembly

Kevin N. Baumann[1], Luca Piantanida[2†], Javier García-Nafría[3‡], Diana Sobota[4], Kislon Voïtchovsky[2], Tuomas P. J. Knowles[1,4], Silvia Hernández-Ainsa[5,6,7*]*

[1]University of Cambridge, Department of Chemistry, Lensfield Road, CB2 1EW, Cambridge, United Kingdom

[2]University of Durham, Department of Physics, Durham DH1 3LE, United Kingdom

[3]MRC Laboratory of Molecular Biology, CB2 0QH, Cambridge, United Kingdom

[4]University of Cambridge, Cavendish Laboratory, CB3 0HE, Cambridge, United Kingdom

[5]Instituto de Nanociencia de Aragón, Universidad de Zaragoza, Campus Río Ebro, Edificio I+D, Zaragoza, Spain

[6]Instituto de Ciencia de Materiales de Aragón, Universidad de Zaragoza-CSIC, Zaragoza, Spain

[7]ARAID Foundation, Zaragoza, Spain

KEYWORDS: DNA nanotechnology, biomimetics, liposome, clathrin, atomic force microscopy, cryo-electron microscopy.

ABSTRACT: The self-assembly of the protein clathrin on biological membranes facilitates essential processes of endocytosis in biological systems and has provided a source of inspiration for materials design by the highly ordered structural appearance. By mimicking the architecture of clathrin self-assemblies to coat liposomes with biomaterials, new classes of hybrid carriers can be derived. Here we present a method for fabricating DNA-coated liposomes by hydrophobically anchoring and subsequently growing a DNA network on the liposome surface which structurally mimics clathrin assemblies. Dynamic light scattering (DLS), ζ-potential and cryo-electron microscopy (cryo-EM) measurements independently demonstrate successful DNA coating. Nanomechanical measurements conducted with atomic force microscopy (AFM) show that the DNA coating enhances the mechanical stability of the liposomes relative to uncoated ones. Furthermore, we provide the possibility to reverse the coating process by triggering the disassembly of the DNA coating through a toehold-mediated displacement reaction. Our results describe a straightforward, versatile, and reversible approach for coating and stabilizing lipid vesicles by an interlaced DNA network. This method has potential for further development towards the ordered arrangement of tailored functionalities on the surfaces of liposomes and for applications as hybrid nanocarrier.

MAIN TEXT

The protein clathrin plays a major role in cell trafficking by mediating endocytosis.[1] In its monomeric form, clathrin has the shape of a triskelion. Upon an external stimulus it forms spherical complexes surrounding a membrane vesicle with an alternating pattern of hexagons and pentagons.[2,3] In addition to its biological significance, the structural elegance of clathrin has

inspired the development of artificial functional materials that mimic clathrin lattices and their self-assembly.[4–6]

DNA is increasingly exploited as a building material for predictable and precise assembly of various structures on the nanoscale. DNA nanostructures can be conceived by specifically designing the individual nucleotide sequences, which then form unique shapes aided by the Watson-Crick base-pairing interactions. Furthermore, the choice of DNA as a material allows for multiple biomedical applications due to essential characteristics, such as water-solubility and biodegradability.[7,8] The conjugation of DNA and liposomes has enabled their use as carriers[9,10] or as artificial systems imitating the structure or functionality of certain membrane proteins.[11–15] Many of the so far presented approaches of DNA structures anchored to the liposome surface use spatially uncontrolled attachment.[15–17] The arrangement of DNA structures to supramolecular DNA lattices is still mainly restricted to 2D supported lipid bilayers.[4,18,19] Larger arrangements of DNA assemblies from spatially defined subunits on the surface of a liposome have predominantly employed DNA origami structures.[4,19–21] For instance DNA origami-based rectangles[4] as well as curved DNA origami nanoconstructs[20] have been interconnected on lipid vesicles. Yet, such DNA origami networks were shown to produce liposome deformation or even destruction, which potentially limits the applicability for purposes such as the transport of cargo in vesicles. Moreover, the use of DNA origami constructs in order to achieve dense vesicle coating is a more complex synthetic approach compared to other DNA assemblies based on DNA tiles or junctions.

This study presents a straight-forward method of coating and stabilizing nanoscale lipid vesicles with a semi-rigid DNA network, based on interlaced three-arm branched DNA junctions mimicking the structure of clathrin.

Large unilamellar vesicles (LUVs) were prepared by extrusion of a POPC lipid suspension in phosphate-buffered saline solution (PBS) through a 200 nm pore size membrane.[22] To facilitate coating of the vesicles while reducing DNA aggregation in bulk, a two-step annealing process was applied (Figure 1a). First, LUVs (from now on defined as V) were incubated overnight at room temperature with DNA linkers labelled with a cholesterol tag through a triethylene glycol spacer (Chol-TEG) to render structures referred to as VL (Figure 1a). These linkers were composed of an 18 nucleotides (nt) long DNA duplex containing 18 nt long overhangs on either side (Figure 1b; Supporting Information, Table S1). In the second step, a DNA triskelion (Figure 1c and 1d) was added to the VL structures to achieve the final construct VLT (Figure 1a) through complementary hybridization with the overhangs of the linker via incubation at 4 °C for 50 min. The triskelion consisted of three DNA strands forming a three-arm branched junction (Figure 1c). Three types of triskelion nanostructures (T1, T2 and T3) were prepared which differed by the number of unpaired bases (1, 2 or 3 thymine bases respectively) forming the hinge in the center of the three branches, to study the influence of different mechanical flexibilities on the coating and rigidity of the resulting hybrid structures (VLT1, VLT2, VLT3; Supporting Information, Table S2). Specifically, the 1 thymine hinge (T1 design) was expected to generate the triskelion with the highest rigidity and the 3 thymine bases hinge (T3 design) the most flexible triskelion. This assumption was based on the difference of the persistence lengths and stiffnesses of single-stranded DNA (ssDNA) and double-stranded DNA (dsDNA).[23,24] Their correct assembly was confirmed by atomic force microscopy (AFM) (Figure 1d; Supporting Information, Figure S2) and gel electrophoresis (Supporting Information, Figure S1).

For each step of the assembly process, the changes in size and surface charge were tracked by dynamic light scattering (DLS) and ζ-potential measurements. The size of the liposomes remained

in the same range upon linker incubation (VL, Figure 1e). However, after adding either of the three triskelia, an increase of the hydrodynamic diameter of c.a. 45 nm was observed (VLT1, VLT2 and VLT3, Figure 1e). No size increase was observed when the triskelion was added to V incubated with a linker lacking the Chol-TEG tag (VL-T, Supporting Information, Figure S5a), which demonstrates the importance of the hydrophobic anchor in enabling the coating process. Alternatively, when the cholesterol-modified linker was assembled with the triskelion in the absence of LUVs (LT), aggregation was observed evidencing the role of vesicles in reducing the formation of DNA clusters (Supporting Information, Figure S5c). This indicates that on the one hand the liposomes template the hybrid structure assembly, and on the other hand the cholesterol-bilayer interactions cause the size increase instead of unspecific DNA adsorption. ζ-potential measurements additionally evidenced the occurrence of the coating process: upon addition of the linker, a drop in the ζ-potential was observed from -4 ± 1 mV (for V) to -19 ± 2 mV (for VL). Further incubation with the triskelion (VLT) resulted into an additional decrease down to -31 mV ± 2 mV for VLT1, 31 ± 2 mV for VLT2, and -32 ± 2 mV for VLT3. The ζ-potential of VL-T obtained by incubating V with a linker without the Chol-TEG tag and the T1 triskelion was with -5 ± 1 mV similar to the value obtained for V (-4 ± 1 mV), further highlighting the necessity of the Chol-TEG modification to enable DNA coating.

Cryo-electron microscopy (cryo-EM) was used to directly visualize the successful coating process. In contrast to V (Figure 2a), the completely assembled hybrid structures (VLT) were observed as lipid vesicles surrounded by a corona of filamentous structures (Figure 2b, c, and d) with the three types of triskelia rendering a similar appearance (see also Supporting Information, Figure S7c to e). The state of VL resembled unmodified liposomes, but with the presence of short

spikes and dark spots on the vesicle surface (Supporting Information, Figure S7a) which can be assigned to the linkers on the surface of the liposomes.

After visually confirming the coating process, AFM in liquid was conducted to investigate the mechanical properties of the hybrid structures. We expected the rigidity provided by the triskelion to follow T1>T2>T3 in agreement with the number of unpaired thymine bases in the hinge.[23,24] The hybrid structures were first compared to V and VL by incubating the samples on mica substrates for 1h under the same conditions (details in the experimental section). By contrast to plain POPC LUVs, which spontaneously rupture upon contact with the substrate due to the specific environmental conditions[25] (Figure 3a), VLT conferred significant vesicle stabilization, preventing the coated liposomes from bursting, independently of the triskelion design (VLT1 is shown in Figure 3c, VLT2 and VLT3 in Supporting Information, Figure S10). Topographic measurements by AFM of the hybrid vesicles (profile graph in bottom panel of Figure 3c) indicate an average peak height of approximately 40 nm. This value is lower than the in-solution diameter of the vesicles, a fact that can be explained by the deformation and flattening of the vesicles by the AFM tip during imaging. Since compression by the tip and tip convolution effects are expected, the lateral dimensions of the hybrid vesicles are not reliable for quantification of the size distribution obtained from AFM. V and VL by contrast form a roughly 4 nm thick layer on the substrate (bottom panel, Figure 3a and 3b) matching typical dimensions of lipid bilayers.[26]

Strikingly, a dependence of the mechanical rigidity of VLT on the employed triskelion was observed using AFM. In agreement with the initially hypothesized triskelion rigidity, the Young's modulus values of the hybrid structures follow a trend of VLT1>VLT2>VLT3 (Figure 3d).

Besides the mechanical stabilization, the chemical stability provided by the DNA coating against detergents was probed by treating the samples with 0.5% Triton-X 100 (TX100). The addition of

TX100 completely destroyed V and VL as denoted by the disappearance of the peaks corresponding to the assembled structures obtained from DLS (Figure 4a). The peak centered at approximately 11 nm is observed in all cases and is assigned to the presence of TX100 micelles in solution (Supporting Information, Figure S6a). In contrast, VLT confers a degree of stabilization against the detergent according to the peaks observed by DLS (Figure 4a; Supporting Information Figure S6c and d), matching previous similar observations for other DNA coated liposomes.[27]

We next explored the possibility of making the hybrid structures responsive. Aiming to mimic the function of proteins such as Hsc70 in mediating clathrin-disassembly and dissociation from liposomes[28,29], the T1 DNA triskelion was engineered to allow for a toehold displacement-triggered disintegration of the DNA mesh on the lipid vesicle surface (Figure 4b). The distance where linker and triskelion hybridized was shortened to 12 bp and a 10 nt toehold was introduced (Figure 4b; Supporting Information, Table S4). The resulting hybrid structure, referred to as VLT1s, showed a hydrodynamic diameter of 246 ± 13 nm, agreeing with the previously described VLT1, VLT2 and VLT3 structures. Upon addition of a displacement strand (S), the average size decreased to 195 ± 5 nm (Figure 4c), a value similar to that obtained for uncoated liposomes. This observation, together with the ζ-potential increase from -31 ± 2 mV to -22 ± 1 mV, measured after the addition of S, indicate the successful removal of the DNA coating. Further evidence of the disassembly was provided by tracking the fluorescence quenching upon the hybridization of S labelled with a Black Hole II quencher and the triskelion, labelled with ATTO 590N (Supporting Information, Figure S13). Sequentially to the dissociation by incubation with S, the coating could be reinstated by adding the original TS1 triskelion to the beforehand uncoated vesicles as denoted by a size increase back to 238.0 ± 7 nm (Figure 4c). In agreement with the response of V, VL, and VLT to the presence of TX100, the still coated hybrid structure VLT1s was detectable upon TX100

addition as indicated by a peak in DLS positioned at the original size (Figure 4c, bottom row), whereas the VLT1s vesicles incubated with S were destroyed by the detergent (no peak at original position). The enhanced stability against TX100 treatment could be reestablished by adding T1 to the formerly uncoated VLT1s (in absence of TX100, Figure 4c).

Notably, cryo-EM was able to verify the success of the disassembly process by visualizing the coated (VLT1s) and uncoated state (VLT1s + S). Indeed, whereas VLT1s contained a DNA mesh as observed before (Figure 2b to d) on the vesicle surface (Figure 4d, left image; Supporting Information, Figure S8a to c), the addition of S resulted into the reduction of the DNA corona (Figure 4d, right image; Supporting Information, Figure S8d and e).

In conclusion, we have described a straightforward approach to generate a DNA coating inspired by clathrin self-assembly with enhanced mechanical stability and reduced detergent solubilization of POPC liposomes. We demonstrate that the DNA coating can be designed to be disassembled through a toehold-mediated displacement reaction and further reassembled by the subsequent addition of a DNA triskelion as proposed. The DNA coating could be further derivatized to equip liposomes with a variety of functionalities. This possibility is of interest for several purposes including drug delivery, since these hybrid structures possess the carrier capabilities provided by liposomes as well as the functionality, stability, and programmability of the surrounding DNA network.

Experimental Section

Liposome preparation

LUVs were prepared as previously described[22] by extruding a solution of 2 mM POPC in PBS through 200 nm extrusion membranes purchased from Avanti Lipids. POPC was bought as powder from Sigma Aldrich and diluted to a 200 mM stock in chloroform.

DNA triskelion folding and characterization

DNA oligonucleotides were purchased from Integrated DNA Technologies Inc (IDT). Linker and triskelion were assembled in PBS and subjected to the thermal programs described in the Supporting Information (section S1). The linker was assembled at 4 μM concentration (by the equimolar mixture of the two strands) and the triskelion at a 6 μM concentration (by the equimolar mixture of the three strands). Successful folding was assessed polyacrylamide gel electrophoresis (PAGE, details in Supporting Information S2) and AFM.

Assembly and disassembly of the DNA coating on liposomes

The hybrid structures were prepared by first incubating the linker (added at 3 μM) overnight at room temperature with the vesicle solution (2 mM POPC) resulting in a linker concentration of 1.1 μM and POPC concentration of 1.2 mM. Subsequently, the triskelion was added to the mixture (at 4 μM) and incubated for 50 min at 4 °C. The final mixture contained 1 mM POPC lipids, 930 nM linker, and 620 nM triskelion.

For the toehold-mediated coating disassembly, the T1s triskelion was employed. T1s was designed with shorter complementary domains (12 bp) and a 10 nt long toehold to allow for displacement by an added fully complementary 22 nt long displacement strand (S). Liposome coating was performed as described above to yield VLT1s. S was added to the VLT1s solution at twice the concentration of toeholds present in T1s and incubated for 10 minutes at 4 °C to achieve the disassembly of the DNA coating (VLT1sS). The reassembly process was carried out with the T1 triskelion following the same protocol for the respective incubation step as described above.

Hydrodynamic diameter and zeta potential measurement

Hydrodynamic diameters and ζ-potential were measured with a ZetaSizer Nano ZSP by Malvern Panalytics. All liposome-containing samples were measured at a final lipid concentration of 1 mM in PBS. The untreated vesicles (V) were measured after being diluted 1:1 in PBS (total volume 100 μL) to match the concentration of the hybrid structures. The vesicles with linkers (VL) were measured by topping up the aliquots to 100 μL with PBS for the same reason. The final hybrid vesicles (VLT) were measured directly. The reported results show average values of three preparations for each sample (V, VL, VLT). Controls involved LT1 (incubation without vesicles), VL-T (linker without Chol-TEG), $VLT_{no\text{-}match}$ (incubated with a T1-based triskelion having non-hybridizing sticky ends) and VT (liposomes and the T1 triskelion without the linker).

Cryo-electron microscopy

Cryo-EM grids were prepared by applying 3 μL of sample (at 1 nM concentration) on glow discharged holey grids (Quantifoil Cu 1.2/1.3 400 mesh). Excess sample was removed by blotting

with filter paper for 4 sec prior to plunge-freezing in liquid ethane using a FEI Vitrobot Mark IV at 100% humidity and 4 °C. Data was collected on a FEI Tecnai F20 FEG microscope at 200 kV using a Falcon II (or Falcon III) direct electron detector (always in linear mode). Images were collected at a dose rate of $20e^-$/pixel/second with a total dose of $40e^-/Å^2$. Magnification was set to 50,000x yielding a pixel size of 2.08Å/pixel at the specimen level.

Atomic force microscopy and force spectroscopy

Samples were prepared placing 20 μL of 25 mM $MgCl_2$ (final concentration 5 mM due to dilution by the samples) onto a freshly cleaved mica followed by 50 μL of the specific sample solution (V, VL, VLT1, VLT2, VLT3) together with 30 μL of 10 mM Tris-HCl (pH = 7.4, final concentration 3 mM). All samples were incubated at room temperature for 1h, followed by the addition of another 20 μL of the 25 mM $MgCl_2$ solution to further promote sample adhesion to the substrate.

Imaging the three triskelion configurations (T1, T2, T3), as well as the combination of linker and T2 triskelion (LT2), was achieved diluting the samples 10 times in 1x TAEM buffer (1x TAE + 25 mM $MgCl_2$, pH = 7.4) and placing 2 μL of the solution on a mica substrate. Subsequently, 10 μL 1x TAEM buffer and 2 μL of a 100 mM $NiCl_2$ solution were added. After a minute equilibration time additional 60 μL of the 1x TAEM buffer were supplemented.

A commercial Cypher ES AFM (Asylum Research) equipped with direct laser excitation (blueDrive) and temperature control was used for all experiments. Imaging was carried out in amplitude modulation (AM) with the cantilever fully immersed in liquid and at a controlled temperature of 25 ± 0.1 °C. As in standard AM operation, the cantilever was driven at its

fundamental resonance frequency and the amplitude kept constant while scanning. The cantilever used for all the LUVs analysis (OMCL RC800-PSA, Olympus, Tokyo, Japan) had a nominal spring constant of 0.05 N/m. During imaging, the set-point ratio $S = A/A_0$ between the imaging amplitude A and free amplitude A_0 was kept as high as possible (typically $S > 0.8$) to limit the force applied to the vesicles. For the linker and triskelion analysis, we used a cantilever with a nominal spring constant of 0.38 N/m (ORC8, Bruker, Camarillo, US), keeping a set-point ratio of $S \sim 0.7$. All the images were corrected for tilt (line or plane flattening) and lightly low-pass filtered to remove grainy noise using the WSxM software (Nanotec Electronica, Madrid, Spain)[30].

For the quantification of the Young's moduli from spectroscopy measurements, averaged data from at least 10 force curves (FCs) for each sample (VLT1, VLT2, VLT3) were analyzed using custom routines programmed in Igor Pro (WaveMetrics, Lake Oswego, USA). The Young's modulus was calculated by fitting a suitable region of the FCs using a previously described equation[31] for analyzing vesicular structures.

FIGURES

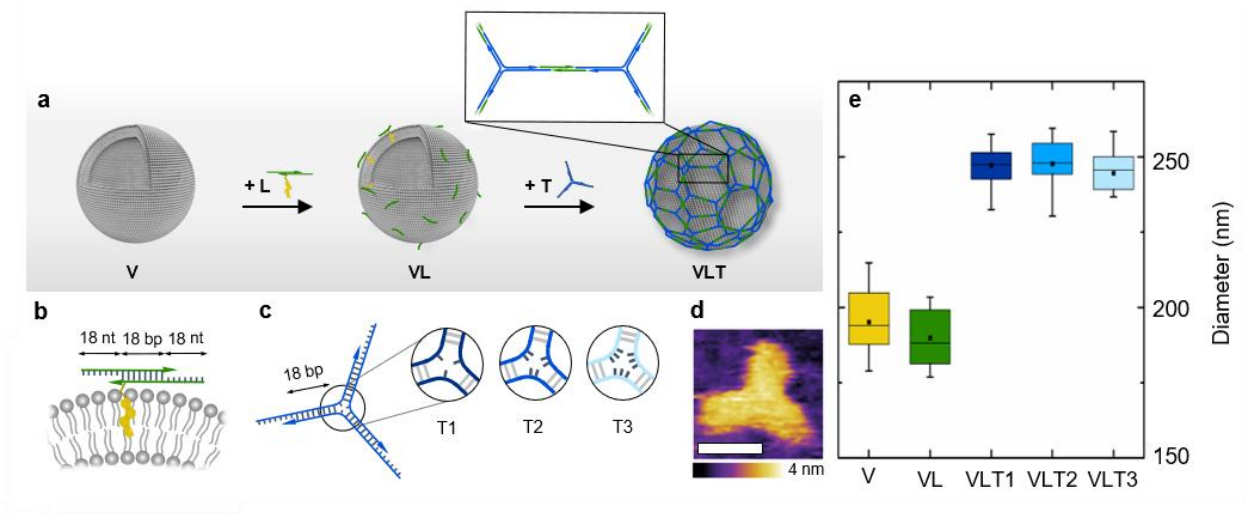

Figure 1. (a) Two-step assembly process where the linker attaches first to the vesicles, and the triskelion hybridizes subsequently to form a network on the vesicle surface (not to scale). (b) Representation of the linker attached to a liposome through a Chol-TEG tag at the 3'-end of one of the oligonucleotides composing the duplex. 18 nt long overhangs were included on each side of the linker to anneal with the triskelion. (c) Representation of the triskelion with a complementary 18 nt overhang per arm to hybridize with the linker. The three configurations T1, T2, T3 differ by the number of unpaired thymine bases in the hinge. (d) AFM micrograph of the T1 triskelion in liquid. Lateral scale bar: 10 nm. (e) Hydrodynamic diameters of the different hybrid structures obtained by DLS with V = 195 ± 10 nm, VL= 190 ± 9 nm, VLT1 = 247 ± 6 nm, VLT2 = 248 ± 8 nm, and VLT3 = 245 ± 7 nm (from counts in intensity). The stated values represent the averages and the standard deviations of 5 measurements of 3 independent sample preparations each.

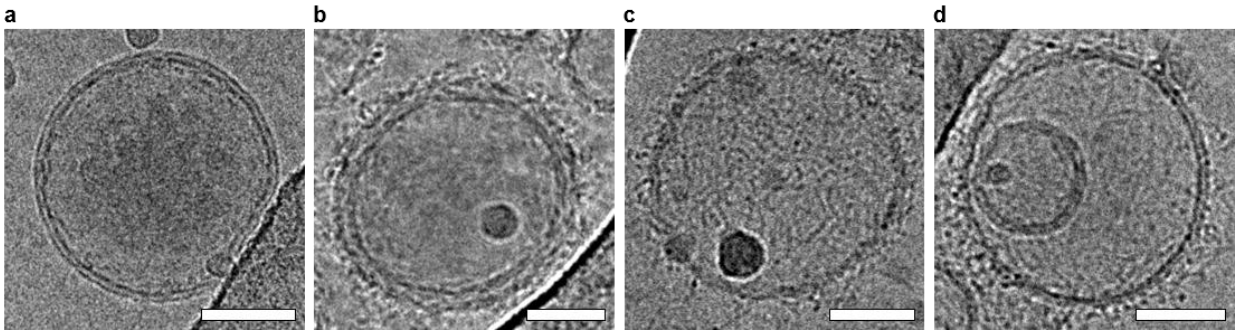

Figure 2. Cryo-EM images of V (a), VLT1 (b), VLT2 (c), and VLT3 (d). When coating the vesicles, an interlaced filamentous DNA network can be seen surrounding the vesicles. Scale bars: 50 nm.

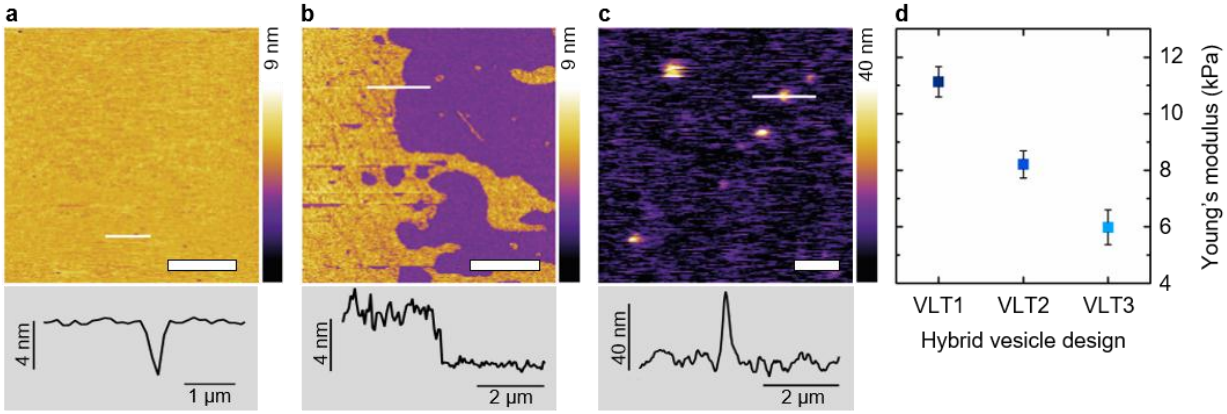

Figure 3. AFM in liquid shows a stabilizing influence of the DNA coating on the LUVs. Topographic AFM images in liquid and selected height profiles of (a) V (lateral scale bar: 2.5 µm), (b) VL (lateral scale bar: 2.5 µm) and (c) VLT1 (lateral scale bar: 1 µm). The white lines in the images indicate the positions of the line profiles plotted in the bottom panels. (d) Young's moduli of the three configurations of coated vesicles in dependence of the involved triskelion design (VLT1: 11.1 ± 0.5 kPa, VLT2: 8.2 ± 0.5 kPa, VLT3: 6.0 ± 0.6 kPa). Error bars correspond to the standard error of the mean of 10 measurements per hybrid vesicle design.

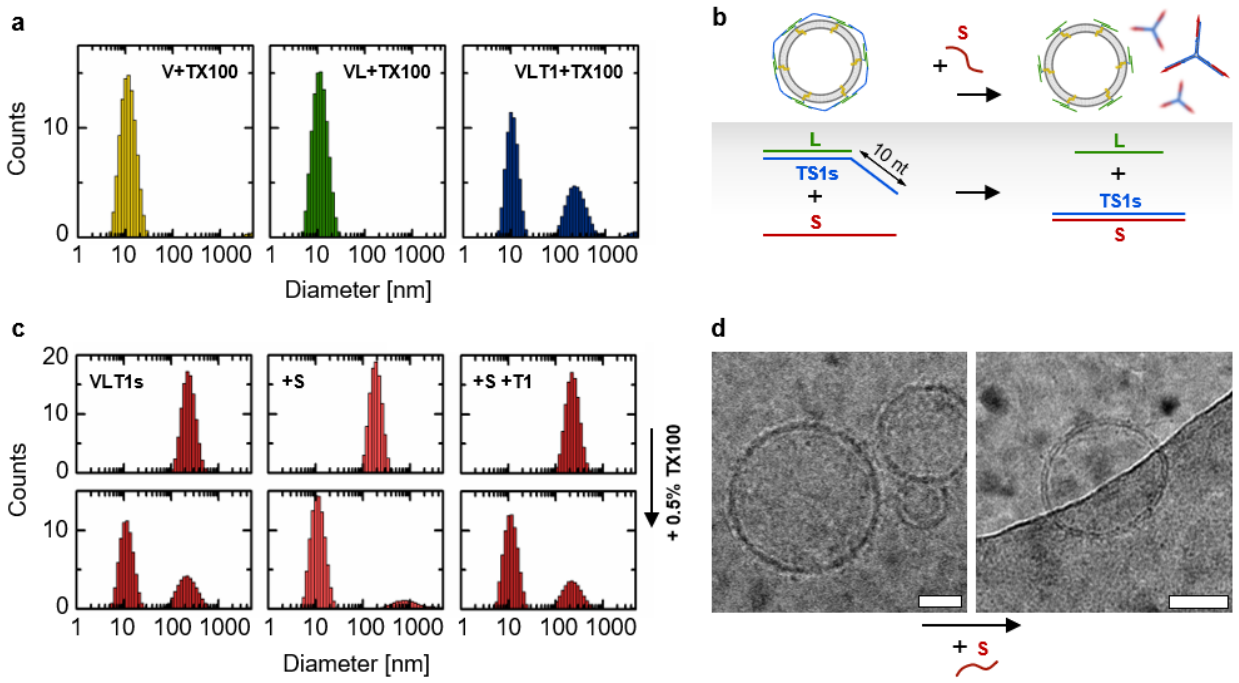

Figure 4. Chemical resistance of the hybrid structures and reversibility of the vesicle coating process. (a) Hydrodynamic diameters of V, VL and VLT1 samples after addition of TX100 obtained from DLS (counts in intensity). (b) Schematic representation of the VLT1s disassembly through a toehold-mediated displacement reaction. A 10 nt toehold was included in the T1 triskelion (thus referred to T1s) hybridizing with a displacement strand S. (c) Top panels: size (hydrodynamic diameters by DLS from counts in intensity) of VLT1s before and after the addition of S, and the subsequent addition of the original T1. The bottom panels collect the DLS data of each sample upon addition of 0.5% TX100. (d) Cryo-EM images of VLT1s before (left) and after addition of S (right). Scale bars: 50 nm.

AUTHOR INFORMATION

Corresponding Authors

* Silvia Hernández-Ainsa: silviamh83@unizar.es

* Tuomas P. J. Knowles: tpjk2@cam.ac.uk

Present Addresses

† INSERM U1067, Adhesion and Inflammation Lab, 163 Avenue de Luminy, 13009 Marseille, France

‡ Institute of Biocomputation and Physics of Complex Systems (BIFI), University of Zaragoza, BIFI-IQFR (CSIC), 50018, Zaragoza, Spain

Author Contributions

The manuscript was written through contributions of all authors. All authors have given approval to the final version of the manuscript.

Funding Sources

The research leading to these results has received funding from the European Research Council under the European Union's Seventh Framework Programme (FP7/2007-2013) through the ERC grant PhysProt (agreement n° 337969). KNB and TPJK are grateful for financial support from the Biotechnology and Biological Sciences Research Council (BBSRC), the Newman Foundation, the Wellcome Trust and the Cambridge Centre for Misfolding Diseases. KV and LP acknowledge funding from the BBSRC (grant BB/M024830/1). JGN receives support from Heptares

Therapeutics. DS is supported by the Winton Trust for Sustainable Physics. SHA acknowledges funding by the University of Zaragoza (UZ2018-CIE-04 and JIUZ-2018-CIE-04).

ACKNOWLEDGMENT

The authors would like to thank Magdalena A. Czekalska, Dr. Jinbo Zhu, Prof. Ulrich Keyser and Dr. Lorenzo Di Michele for insightful discussions.

ABBREVIATIONS

Cryo-EM, cryo-electron microscopy; AFM, atomic force microscopy; DLS, dynamic light scattering; DNA, deoxyribonucleic acid; ssDNA, single-stranded DNA; dsDNA, double-stranded DNA; PAGE, polyacrylamide gel electrophoresis; AGE, agarose gel electrophoresis; LUV, large unilamellar vesicle.

REFERENCES

(1) McMahon, H. T.; Boucrot, E. Molecular Mechanism and Physiological Functions of Clathrin‐Mediated Endocytosis. *Nat. Publ. Gr.* **2011**, *12* (8), 517–533.

(2) Heuser, J. E.; Keen, J. H.; Amende, L. M.; Lippoldt, R. E.; Prasad, K. Deep-Etch Visualization of 27S Clathrin: A Tetrahedral Tetramer. *J. Cell Biol.* **1987**, *105* (5), 1999–2009.

(3) Kaksonen, M.; Roux, A. Mechanisms of Clathrin-Mediated Endocytosis. *Nat. Rev. Mol. Cell Biol.* **2018**, *19* (5), 313–326.

(4) Kocabey, S.; Kempter, S.; List, J.; Xing, Y.; Bae, W.; Schiffels, D.; Shih, W. M.; Simmel,

F. C.; Liedl, T. Membrane-Assisted Growth of DNA Origami Nanostructure Arrays. *ACS Nano* **2015**, *9* (4), 3530–3539.

(5) Vitaliano, G. D.; Vitaliano, F.; Rios, J. D.; Renshaw, P. F.; Teicher, M. H. New Clathrin-Based Nanoplatforms for Magnetic Resonance Imaging. *PLoS One* **2012**, *7* (5), e35821.

(6) Kong, Y.; Hanna, M. E. S.; Zhuo, D.; Chang, K. G.; Bozorg-Grayeli, T.; Melosh, N. A. Self-Assembly of Mesoscale Artificial Clathrin Mimics. *ACS Nano* **2017**, *11* (10), 9889–9897.

(7) Kumar, V.; Palazzolo, S.; Bayda, S.; Corona, G.; Toffoli, G.; Rizzolio, F. DNA Nanotechnology for Cancer Therapy. *Theranostics* **2016**, *6* (5), 710–725.

(8) Jiang, Q.; Zhao, S.; Liu, J.; Song, L.; Wang, Z.; Ding, B. Rationally Designed DNA-Based Nanocarriers. *Adv. Drug Deliv. Rev.* **2019**, *In press*.

(9) Lopez, A.; Liu, J. DNA Oligonucleotide-Functionalized Liposomes: Bioconjugate Chemistry, Biointerfaces, and Applications. *Langmuir* **2018**, *34* (49), 15000–15013.

(10) Banga, R. J.; Chernyak, N.; Narayan, S. P.; Nguyen, S. T.; Mirkin, C. A. Liposomal Spherical Nucleic Acids. *J. Am. Chem. Soc.* **2014**, *136* (28), 9866–9869.

(11) Göpfrich, K.; Zettl, T.; Meijering, A. E. C.; Hernández-Ainsa, S.; Kocabey, S.; Liedl, T.; Keyser, U. F. DNA-Tile Structures Induce Ionic Currents through Lipid Membranes. *Nano Lett.* **2015**, *15* (5), 3134–3138.

(12) Göpfrich, K.; Li, C.-Y.; Ricci, M.; Bhamidimarri, S. P.; Yoo, J.; Gyenes, B.; Ohmann, A.; Winterhalter, M.; Aksimentiev, A.; Keyser, U. F. Large-Conductance Transmembrane

Porin Made from DNA Origami. *ACS Nano* **2016**, *10* (9), 8207–8214.

(13) Langecker, M.; Arnaut, V.; Martin, T. G.; List, J.; Renner, S.; Mayer, M.; Dietz, H.; Simmel, F. C. Synthetic Lipid Membrane Channels Formed by Designed DNA Nanostructures. *Science.* **2012**, *338* (6109), 932–936.

(14) Xu, W.; Wang, J.; Rothman, J. E.; Pincet, F. Accelerating SNARE-Mediated Membrane Fusion by DNA-Lipid Tethers. *Angew. Chemie - Int. Ed.* **2015**, *54* (48), 14388–14392.

(15) Ohmann, A.; Li, C.-Y.; Maffeo, C.; Al Nahas, K.; Baumann, K. N.; Göpfrich, K.; Yoo, J.; Keyser, U. F.; Aksimentiev, A. A Synthetic Enzyme Built from DNA Flips 107 Lipids per Second in Biological Membranes. *Nat. Commun.* **2018**, *9* (1), 2426.

(16) Langecker, M.; Arnaut, V.; List, J.; Simmel, F. C. DNA Nanostructures Interacting with Lipid Bilayer Membranes. *Acc. Chem. Res.* **2014**, *47* (6), 1807–1815.

(17) Wu, N.; Chen, F.; Zhao, Y.; Yu, X.; Wei, J.; Zhao, Y. Functional and Biomimetic DNA Nanostructures on Lipid Membranes. **2018**, *34*, 14721–1430.

(18) Avakyan, N.; Conway, J. W.; Sleiman, H. F. Long-Range Ordering of Blunt-Ended DNA Tiles on Supported Lipid Bilayers. *J. Am. Chem. Soc.* **2017**, *139* (34), 12027–12034.

(19) Suzuki, Y.; Endo, M.; Sugiyama, H. Lipid-Bilayer-Assisted Two-Dimensional Self-Assembly of DNA Origami Nanostructures. *Nat. Commun.* **2015**, *6*, 8052.

(20) Schwille, P.; Dietz, H. Membrane Sculpting by Curved DNA Origami Scaffolds. *Nat. Commun.* **2018**, *9* (1), 811.

(21) Suzuki, Y.; Endo, M.; Yang, Y.; Sugiyama, H. Dynamic Assembly/Disassembly Processes

of Photoresponsive DNA Origami Nanostructures Directly Visualized on a Lipid Membrane Surface. *J. Am. Chem. Soc.* **2014**, *136* (5), 1714–1717.

(22) Hernández-Ainsa, S.; Ricci, M.; Hilton, L.; Aviñó, A.; Eritja, R.; Keyser, U. F. Controlling the Reversible Assembly of Liposomes through a Multistimuli Responsive Anchored DNA. *Nano Lett.* **2016**, *16* (7), 4462–4466.

(23) Chi, Q.; Wang, G.; Jiang, J. The Persistence Length and Length per Base of Single-Stranded DNA Obtained from Fluorescence Correlation Spectroscopy Measurements Using Mean Field Theory. *Physica A* **2013**, *392* (5), 1072–1079.

(24) Brunet, A.; Tardin, C.; Salomé, L.; Rousseau, P.; Destainville, N.; Manghi, M. Dependence of DNA Persistence Length on Ionic Strength of Solutions with Monovalent and Divalent Salts: A Joint Theory–Experiment Study. *Macromolecules* **2015**, *48* (11), 3641–3652.

(25) Hardy, G. J.; Nayak, R.; Zauscher, S. Model Cell Membranes: Techniques to Form Complex Biomimetic Supported Lipid Bilayers via Vesicle Fusion. *Curr. Opin. Colloid Interface Sci.* **2013**, *18* (5), 448–458.

(26) Lewis, B. A.; Engelman, D. M. Lipid Bilayer Thickness Varies Linearly with Acyl Chain Length in Fluid Phosphatidylcholine Vesicles. *J. Mol. Biol.* **1983**, *166* (2), 211–217.

(27) Ruysschaert, T.; Paquereau, L.; Winterhalter, M.; Fournier, D. Stabilization of Liposomes through Enzymatic Polymerization of DNA. *Nano Lett.* **2006**, *6* (12), 2755–2757.

(28) Schlossman, D. M.; Schmid, S. L.; Braell, W. A.; Rothman, J. E. An Enzyme That Removes Clathrin Coats: Purification of an Uncoating ATPase. *J. Cell Biol.* **1984**, *99* (2), 723–733.

(29) Ungewickell, E.; Ungewickell, H.; Holstein, S. E. H.; Lindner, R.; Prasad, K.; Barouch, W.; Martini, B.; Greene, L. E.; Eisenberg, E. Role of Auxilin in Uncoating Clathrin-Coated Vesicles. *Nature* **1995**, *378* (6557), 632–635.

(30) Horcas, I.; Fernández, R.; Gómez-Rodríguez, J. M.; Colchero, J.; Gómez-Herrero, J.; Baro, A. M. WSXM: A Software for Scanning Probe Microscopy and a Tool for Nanotechnology. *Rev. Sci. Instrum.* **2007**, *78* (1), 13705.

(31) Laney, D. E.; Garcia, R. A.; Parsons, S. M.; Hansma, H. G. Changes in the Elastic Properties of Cholinergic Synaptic Vesicles as Measured by Atomic Force Microscopy. *Biophys. J.* **1997**, *72* (2), 806–813.